mmWave Frequency Reconfigurable Low Noise Amplifiers for 5G

Rana A. Shaheen, Timo Rahkonen and Aarno Pärssinen

***Abstract*— In this brief, designs of two millimeter wave (mmWave) reconfigurable multi band low noise amplifiers (LNA) are presented targeted for fifth generation (5G) communications. A reconfigurable tunable load based on electrical and magnetic tuning is proposed to cover three mmWave frequency bands for 5G, i.e. 24 GHz, 28 GHz and 39 GHz. Two LNA structures are designed and fabricated using 45nm CMOS SOI technology. The first toplogy (LNA1) is composed of a single input wideband matching circuit to cover frequency operations from 24 GHz to 40 GHz. On the other hand, second topology (LNA2) uses three separate narrowband match inputs, one for each frequency band, with combined output. Design methodology of passive and active devices is presented towards compact integration of LNAs for systems such as, phased arrays. Ground plane and its impact on the performance parameters is also discussed in this work. Measurement results show a wideband noise figure (NF) ranging from 3.8 dB to 4.9 dB and gain of 8.5 dB to 12.5 dB for LNA1 at different bands. Similarly, LNA2 exhibits NF of 4.5 dB to 5.5 dB and gain of 9.5 dB to 15.5 dB across all bands. Total area (including pads) of LNA1 and LNA2 are 0.316 mm^2 and 0.695 mm^2, respectively.**

***Keywords*— mm-wave, 5G, multi band, RF, LNA, receiver, reconfigurable, CMOS, SOI.**

I. Introduction

5G New radio (NR) standard released by third generation partnership project (3GPP) has allocated several mmWave frequency bands for 5G systems between 24 GHz to 40 GHz, named as n257, n258, n260 and n261 [1]. Depending on the infrastructure regulations across the globe, mmWave 5G systems use different NR bands in different regions. With the existence of multi-band scenario (similar to LTE), a reconfigurable multi mode radio front-end hardware solution is needed for infrastructure and mobile handsets vendors.

In a frequency reconfigurable phased array receiver system, low noise amplifier (LNA) is the most crcitical circuit block in terms of input matching, noise figure and gain flatness across all frequency bands. Additional design limitations for active and passive devices at mmWave frequencies make it more challenging to design reconfigurable LNA for those frequency bands. Below 6 GHz, prior circuit techniques for multi mode systems include a dedicated input and/or output for multiple wireless standards [2], [3].

In this brief, circuit implementation techniques are discussed to align the key requirements towards mmWave reconfigurable multi-band LNAs. Common approach at mmWave LNA's is to use truly broadband circuits as in [4] and [5]. However, lack of band sepecific filtering make them susceptible to out-of-band interference. Four possible circuit topologies to design a frequency reconfigurable LNA (FR-LNA) are shown in Fig. 1. A wideband input match with tunable resonance load offers a single input single output approach (Fig. 1a). Option two (Fig. 1b) is also based on a single input and single output architecture. However, a tunable matching component that tunes narrowband impedance matching for different frequency bands brings extra switching loss at the input which increases noise figure of the system. Architecture shown in Fig. 1c uses separate input matching circuits for individual frequency bands. However, this architecture has a limitation in terms of larger footprint. A multiple input and multiple output architecture is shown in Fig. 1d, where an individual output load resonator is used for each frequency band. Circuit topologies in Figs. 1c and 1d have larger area. However, they offer better filtering and narrowband input matching for each frequency input towards seamless integration with individual antenna for each frequency band.

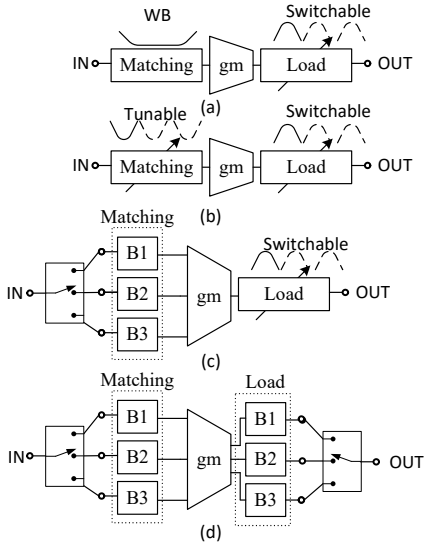

Fig. 1. Reconfigurable LNA circuit techniques

Two mmWave FR-LNA structures based on topologies given in Figs. 1a and 1c, are designed and presented in this paper. Both FR-LNAs are designed to operate at three mmWave frequency bands for 5G, i.e. 24 GHz, 28 GHz and 38 GHz. Section II describes the design of wide tuning range LC resonant load. Design techniques of two LNA

The authors would like to thank Nokia Corporation for financial support and Global Foundries for support in process technology. Matti Polojarvi, Alok and Rehman are highly acknowledged for their support during design and Lab measurements. This research has been also in part financially supported by Academy of Finland 6Genesis Flagship (grant 318927).

Timo Rahkonen and Aarno Parssinen are with University of Oulu, Oulu, Finland (timo.rahkonen@oulu.fi; aarno.parssinen@oulu.fi). Rana A. Shaheen was affiliated with University of Oulu. He is currently with NXP Semiconductor, Caen, France (ranaazhar.shaheen@nxp.com)

structures are discussed in section III. Measurement results with observations are presented in section IV. Section V concludes the work.

II. Tunable LC Resonator

Resonance frequency of an LC resonator can be varied either by capacitance tuning, inductance tuning or both. Capacitance tuning can be implemented either using varactors or switched capacitors (SC). Due to the smaller tuning ratio, varactors are only useful for fine-step tuning. While switched capacitors (SC) can provide coarse or fine tuning. However, metal oxide semiconductor (MOS) switches have more restrictions at mmWave frequencies due to limited quality factor and large ON resistance and OFF capacitance. Therefore, in addition to capacitance tuning, use of inductive tuning is preferred where frequency tuning range can be large. Millimeter wave (mmWave) tunable inductor structures have been previously used and demonstrated in voltage controlled oscillators (VCO) [6], [7], [8].

A wide tuning range LC resonator based on inductive and capacitive tuning is proposed in this work. Proposed tunable resonator is composed of a variable inductor and a switched capacitor bank. The loss of the resonator is optimized for minimum variation between the switching states.

A. Magnetically Tuned Variable Inductor

Inductance can be varied by varying the field strength (i.e. current) or the area covered by the induced magnetic field of an inductor. In silicon based planar structures, a metal ground shield is used around inductor or passive structures to avoid unwanted coupling from surrounding structures, as shown in Fig. 2(a). Current is induced to ground as a result of current flow in the main coil. Intensity of this induced current depends on the strength of coupling (k) between the ground ring and the main coil. The value of k is a strong function of the distance (d) between the two conductors. Inductance of ground coil (L_G), metal resistance of L_G and mutual inductance (M) between the main and ground coils affect the total inductance (L_{tot}) of the structure as given by equation (1) [7],

$$L_{tot} = L_{main} - \frac{\omega^2 M^2 L_G}{R_G^2 + \omega^2 L_G^2}, \tag{1}$$

Induced current in the ground shield exhibits finite resistance due to the conductive losses of the metal. This metal resistance results in a finite quality factor of ground coil (Q_G) which affects the total quality factor of the structure (Q_{tot}) as shown in (2),

$$Q_{tot} = \frac{1 - k^2}{1/Q_{main} + k^2/Q_G}, \tag{2}$$

where coupling factor (k) is defined as,

$$k = \frac{M}{\sqrt{L_{main} L_G}}, \tag{3}$$

A single turn coil with a ground shield structure is designed with fixed radius r using thick copper layer of 45nm

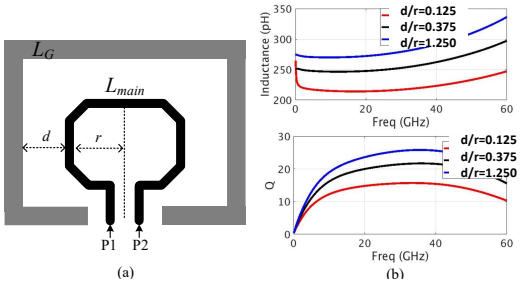

Fig. 2. Ground shield inductor and EM simulation results (a) Layout of inductor with metal ground shield with distance d (b) Inductance (c) Quality factor

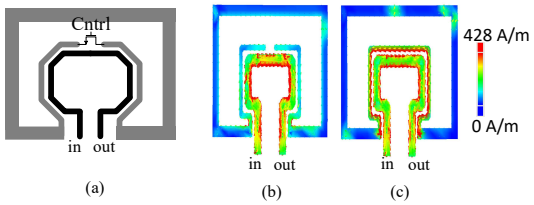

Fig. 3. Variable Inductor (a) Layout of variable inductor (b) 3D visualization of simulated currents at 30 GHz in open and (c) short inner ring, respectively

SOI technology as shown in Fig. 2a. The structure is simulated with three different values of d/r ratio using 2.5D electromagnetic (EM) simulation tool. Variation in quality factor and inductance of the main coil against three different values of d/r are plotted in Fig. 2b. It can be seen that the effect of the ground shield on the inductance and Q of the main coil are the largest when d/r is smaller, i.e.$d<r$ or the k is maximum.

The dependence of ground shield conductor on the inductance value can be used in designing a variable inductor if the distance d can be controlled. A structure is proposed in this work, where the ground shield ring can be switched in two states with the help of a MOS switch, as shown in Fig. 3a. Figs. 3b and 3c show a 3D visualization of induced currents (at 30 GHz) in the ground structure when the path of inner ring is open (high L) and closed (low L), respectively. Metal resistance of the inner ground ring and the ON resistance of the MOS switch have a significant impact on the Q of the main coil. Therefore, a trade off always exists in this structure between the amount of variation in L and Q.

B. Variable LC resonator

A wide tuning range resonance tank circuit composed of a variable inductor (L_{var}) and switched capacitor (SC) bank with their corresponding control bits is shown in Fig. 4a.

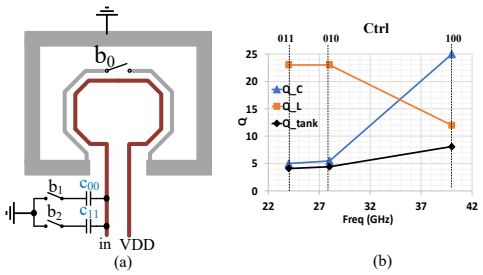

Fig. 4. Variable resonator tank circuit (a) Implementation of variable resonator using variable inductor and switched capacitors with control bits (b) Quality factors of capacitor bank, inductor and tank at three control values

Simulated quality factors of L_{var}, SC bank and tank are plotted against three frequency selecting control words and shown in Fig. 4b. Each control bit controls the NMOS switch with value '1' for ON state and '0' for off state of the switch.

For 40 GHz band selection (control word 100), coil control bit (b_0) is turned on (L_{var} is minimum) while capacitances are turned off, which results in minimum value of Q_{Lvar} and maximum value for Q_{SC} (mainly parasitic capacitance of SC bank). For 28 GHz band selection, coil switch is turned off (L_{var} is maximum) and only b_1 is switched on (C_{00} is added). This leads to maximum value for Q_{Lvar} while Q_{SC} is reduced. Furthermore, by turning on b_2, more capacitance (C_{11}) is added in the circuit for 24 GHz band (control word 011), at the cost of further degradation in Q_{SC}. Above mentioned control selection strategy helps to minimize the variation in total quality factor of the tank (Q_{tank}) across all frequency bands as shown in Fig. 4b (black curve). Having both inductor and capacitor switches on at the same time would lead to very low Q and lack of any proper filtering in the LNA.

III. Circuit Designs

Two mmWave LNA topologies are selected for implementation of multi-band operation with different input matching strategies as shown in Figs. 1a and 1c. LNA1 uses wideband transformer-based input covering all three frequencies of interest. Correspondingly, LNA2 has three narrowband matched inputs one for each frequency band. Both LNAs use similar tunable resonance load as discussed in Section II. Furthermore, due to better input matching conditions for optimum noise figure, design of both LNAs is based on the classical cascode common-source inductively degenerated topology. A major benefit of these structures is that the primary contributor to their total noise figure comes from the insertion loss of their input matching networks. Moreover, since the tunable load resonator is only implemented after the first amplification, therefore, variation in its quality factor does not harm the overall noise performance. However, any discrepancy in these load resonators will directly affect the gain performance of the LNAs.

A. LNA1

The schematic of the LNA1 is shown in Fig. 5a. Device size (total width) is selected to achieve required value of transconductance (g_m) for the targeted gain. Number of gate fingers (n_f) and width of each finger (W_f) are analysed by simulations for optimized maximum frequency f_{max} of the device. To match the input impedance of the LNA1 for wide range of frequencies, a high-order LC network is required that can resonate out the c_{gs} of the input transistor together with source inductance at multiple frequencies. Lumped-element network in [9] generates a second-order bandpass filter terminated with LNA. However, this solution needs two inductors which require larger chip area and introduce more losses. A transformer based matching network offers a wideband matching solution with a compact size.

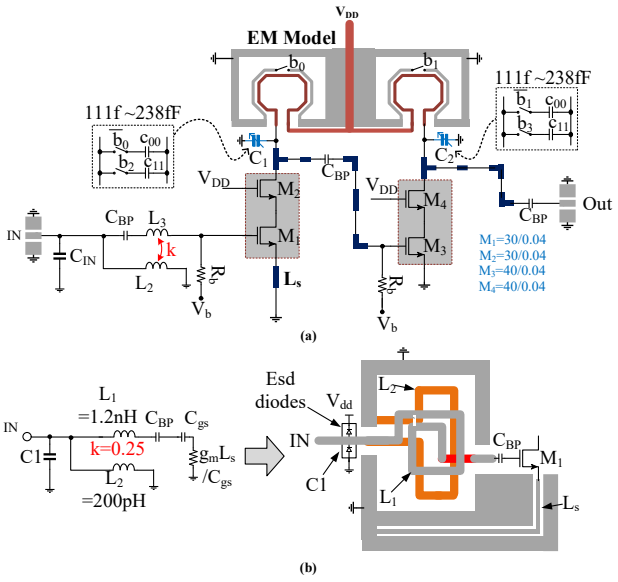

Fig. 5. (a) Schematic of LNA1 (b) Schematic of the wideband input matching technique using transformer and its layout implementation

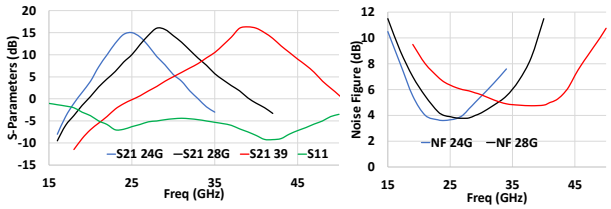

Fig. 6. Simulated S-parameters and noise figure of LNA1 at different band settings (a) S-parameters (b) Noise figure

Therefore, a transformer based input matching network [10] is used for $LNA1$ as shown in Fig. 5a. Values of the components are selected to generate the resonances at 22 GHz and 40 GHz. Input shunt capacitance C1 is realized from the parasitic capacitance of ESD diodes. Layout of the transformer with ground shield ring is also shown in Fig. 5b. Required value of L_1 (1.2 nH) is achieved in 1.5 turns using top aluminum metal (M8) of the technology. L_2 is layed out using M6 under the L_1 to achieve coupling factor of k=0.25. A co-planar wavguide (CPW) transmission line is used as source inductance (L_s).

Variable resonator discussed in Section II is used as the load for two gain stages of the LNA. EM model of two output resonators and power supply distribution network is extracted in from the complete layout. CPW lines are used as interconnects between the active stages. Three frequency bands are reconfigured using four control bits, i.e. $b_0..b_3$. Resonance control for both LNA stages is implemented similarly as described in previous section of variable LC resonator. Simulated s-parameters and noise figure of three frequency band settings are given in Fig. 6 a and b, respectively.

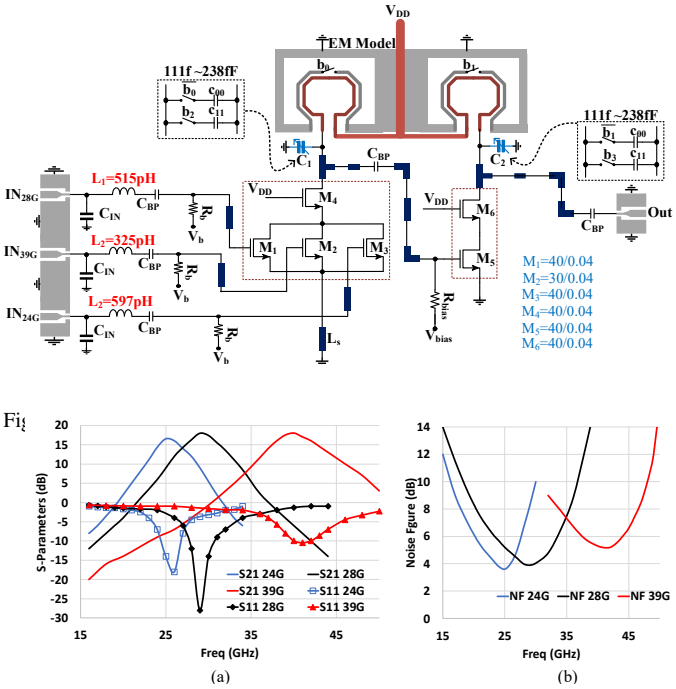

Fig. 8. Simulated S-parameters and noise figure of LNA2 at different band settings (a) S-parameters (b) Noise figure

B. LNA2

In order to provide some selectivity in the input and enable external band specific filtering (Fig. 1c), second LNA shown in Fig. 7 has dedicated input for each band and a single output resonator. Narrowband input noise matching is designed for each band separately with their respective input transistors. Input transistors (M_1-M_3) are connected to a shared cascode transistor M_4. To configure the circuit for a particular frequency band, only respective input transistor is biased to optimum current density and keeping remaining transistors in off-state. Control strategy similar to LNA1 is also used for LNA2. Fig. 8 shows the simulated s-parameters and noise figure for three frequency bands.

IV. Measurement Results

Two mmWave LNAs discussed in section III are designed and fabricated using 45nm CMOS SOI technology by Global Foundries. Micrographs of both LNAs are shown in Fig. 9. Total chip area is 0.18 μm^2 and 0.22 μm^2 for LNA1 and LNA2, respectively. Digital control for biasing and resonance tuning is performed with the help of shift register control logic. Circuits are measured using probes by Cascode technologies. The probes are calibrated upto the tips of the probes. S-parameter measurements are performed using 67 GHz PNA by Keysight. Hot and cold method for measuring NF of the LNAs is determined using 50 GHz Spectrum analyzer by Keysight. Measured NF and s-parameter plots for two frequency configurations of LNA1 are shown in Fig. 10. In low band (LB) operation, LNA1 provides peak gain of 8.5 dB and NF of 3.8 dB at 23 GHz. At high band (HB), i.e. 39 GHz, it provides 12 dB of peak gain and 4.8 dB of NF when configured for high band. Input of the LNA1 shows very good matching for broadband of frequencies (20 GHz to 40 GHz) as shown in Fig. 10

LNA2 has three dedicated input pads for three frequency bands as shown in Fig. 9b. S-parameters and noise figure measurement plots of the LNA2 for three different frequency settings are shown in Fig. 11. For each frequency band, respective input is probed and output is measured from the common output GSG pad. At 24 GHz band, peak gain of 9 dB and noise figure of 5.5 dB is measured. At 28 GHz frequency band, LNA2 provides maximum gain of 11.5 dB and minimum noise figure of 4.9 dB. At 39 GHz frequency mode, LNA2 provides maximum gain of 15.5 dB and minimum noise figure of 5.6 dB.

Measured S21 plots show discrepancy with the simulations at lower frequency bands. During the design process, cascaded simulations were performed using separate extracted models from RC extraction of active devices and EM extraction of passive devices. After investigations it was found that ground return path of switched capacitors was not extracted in simulations properly as a part of the whole layout as shown by red dotted lines in Fig. 12 for LNA1 (also applicable to LNA2 as similar resonator was used in both designs). This results in additional inductance (150 pH) in the ground path which adds up in the resonator when the switched capacitance is turned on. The unwanted inductance moves the corresponding bands (24GHz and 28 GHz) down by 5 to 6 GHz. The problem can be solved with existing model if the switches are connected to vdd instead of ground, that is also validated by EM simulations. However, this requires to change to the PMOS switch, which normally degrades the Q of the switched capacitance banks. Since this discrepancy was found in the load resonator which resulted in the reduced gain. Nevertheless, measured noise figure performance showed good match with the simulations due to the better input matching characteristics.

To the best knowledge of authors, there is no mmWave reconfigurable LNA found in literature. Therefore, performance of this work is compared with the state-of-the-art (SOA) wideband LNAs (Table 1). Despite the switch losses in resonators, the performance of proposed FR-LNAs are comparable with SOA designs in terms of maximum gain and noise figure. Wideband input match of LNA1 provides wideband noise figure equal or lower than dedicated inputs and smaller chip area, which makes this design a suitable choice for broad-band phased array integration. However, LNA2 offers a seamless opportunity to integrate separate antennas or at least antenna feeds for each band.

V. Conclusions

A reconfigurable multiband solution for mmWave receiver front ends is needed in future 5G systems. In this work, two different LNA architectures supporting reconfigurable mmWave multi-band operations are proposed for phased array systems. For resonance tuning, LNAs employ a switchable resonator consisting of a variable inductor together with switched capacitors. LNA1 supports three mmWave frequency

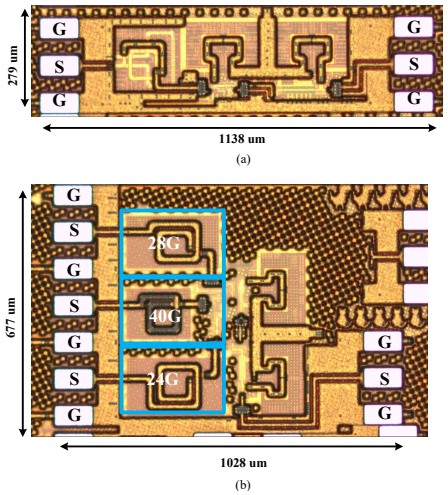

Fig. 9. Micrographs of LNAs (a) LNA1 (b) LNA2

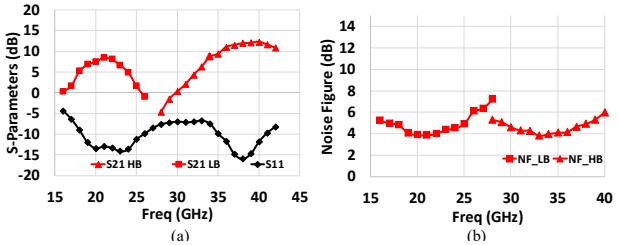

Fig. 10. Measurement results of LNA1 (P_{in}=-30 dBm) (a) S-parameters (b) Noise figure

bands with single input and single output. However, LNA2 is based on three parallel inputs and a single output architecture for multi antenna design. Both designs show noise figure in the range of 3.8 dB to 5.5 dB supporting 24 GHz, 28 GHz and 39 GHz frequency bands for 5G systems. Measured gain of the LNAs varied from 8.5 dB to 15.5 dB across multiple bands. The results indicate that LNAs can be realized using switchable band specific topologies with similar performance compared to broadband counterparts also in the mmWave

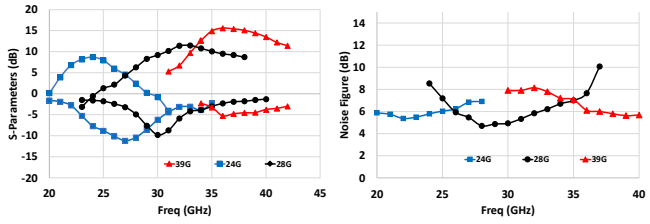

Fig. 11. Measurement results of LNA2 (P_{in}=-30 dBm) (a) S-parameters (b) Noise figure

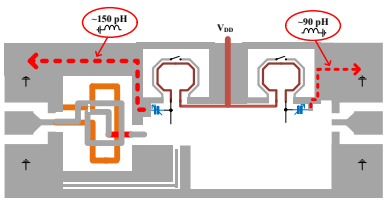

Fig. 12. Layout of passive structures of LNA1 with ground path inductance (dotted red lines)

Table 1. PERFOMRANCE COMPARISON OF LNAs

	This work LNA1	This work LNA2	[4]	[5]	[11]
Process	45nm SOI	45nm SOI	45nm SOI	28nm CMOS	65nm CMOS
Configuration	Multi-band	Multi-band	WB	NB	NB
$Freq$ (GHz)	22/39	24/28/39	24-28	33	24.9-32.5
$Max.Gain$ (dB)	8.5/12.9	9.5/12/15.5	8.5	18.6	18.33
NF (dB)	3.8/4.9	4.5/4.5/5.5	4.0	4.9	3.25-4.2
P_{diss} (mW)	15.5	20.68	12	9.7	20.5
P_{1dB} (dBm)	-11/-16	-12/-13/-16.5	N/A	N/A	-24
$ChipArea$ (mm^2)	0.317	0.69	N/A	0.23	0.11

design.

REFERENCES

[1] 3GPP, "User equipment (ue) radio transmission and reception (release 15)," 3rd Generation Partnership Project (3GPP), Technical Specification (TS), December 2018.

[2] M. Gustafsson, A. Parssinen, P. Bjorksten, M. Makitalo, A. Uusitalo, S. Kallioinen, J. Hallivuori, P. Korpi, S. Rintamaki, I. Urvas, T. Saarela, and T. Suhonen, "A low noise figure 1.2-v cmos gps receiver integrated as a part of a multimode receiver," in *2006 Proceedings of the 32nd European Solid-State Circuits Conference*, Sep. 2006, pp. 78–81.

[3] T. Georgantas and et. al, "9.1 a 13mm2 40nm multiband gsm/edge/hspa+/tdscdma/lte transceiver," in *2015 IEEE International Solid-State Circuits Conference - (ISSCC) Digest of Technical Papers*, Feb 2015, pp. 1–3.

[4] U. Kodak and G. M. Rebeiz, "A 42mw 26–28 ghz phased-array receive channel with 12 db gain, 4 db nf and 0 dbm iip3 in 45nm cmos soi," in *2016 IEEE Radio Frequency Integrated Circuits Symposium (RFIC)*, May 2016, pp. 348–351.

[5] M. Keshavarz Hedayati, A. Abdipour, R. Sarraf Shirazi, C. Cetintepe, and R. B. Staszewski, "A 33-ghz lna for 5g wireless systems in 28-nm bulk cmos," *IEEE Transactions on Circuits and Systems II: Express Briefs*, vol. 65, no. 10, pp. 1460–1464, 2018.

[6] P. Agarwal, S. P. Sah, R. Molavi, S. Mirabbasi, P. P. Pande, S. E. Oh, J. Kim, and D. Heo, "Switched substrate-shield-based low-loss cmos inductors for wide tuning range vcos," *IEEE Transactions on Microwave Theory and Techniques*, vol. 65, no. 8, pp. 2964–2976, Aug 2017.

[7] P. You and T. Huang, "A switched inductor topology using a switchable artificial grounded metal guard ring for wide-ftr mmw vco applications," *IEEE Transactions on Electron Devices*, vol. 60, no. 2, pp. 759–766, Feb 2013.

[8] J. Yin and H. C. Luong, "A 57.5 – 90.1-ghz magnetically tuned multimode cmos vco," *IEEE Journal of Solid-State Circuits*, vol. 48, no. 8, pp. 1851–1861, Aug 2013.

[9] A. Ismail and A. A. Abidi, "A 3-10-ghz low-noise amplifier with wideband lc-ladder matching network," *IEEE Journal of Solid-State Circuits*, vol. 39, no. 12, pp. 2269–2277, Dec 2004.

[10] P. Qin and Q. Xue, "Compact wideband lna with gain and input matching bandwidth extensions by transformer," *IEEE Microwave and Wireless Components Letters*, vol. 27, no. 7, pp. 657–659, July 2017.

[11] S. Kong, H. Lee, S. Jang, J. Park, K. Kim, and K. Lee, "A 28-ghz cmos lna with stability-enhanced gm-boosting technique using transformers," in *2019 IEEE Radio Frequency Integrated Circuits Symposium (RFIC)*, 2019, pp. 7–10.